AIAA 81-0637R

Active Control of Forward-Swept Wings with Divergence and Flutter Aeroelastic Instabilities

Kenneth E. Griffin*
United States Air Force Academy, Colorado Springs, Colorado
and
Franklin E. Eastep†
University of Dayton, Dayton, Ohio

A study is made of simple active control laws to suppress aeroelastic flutter and divergence on forward-swept advanced composite wings. Two selected wing designs are used as examples where leading- and trailing-edge flaps are used as control devices. These flaps are actuated using simple feedback signals from acceleration, velocity, and displacement sensors. The analysis method uses root locus plots of the characteristic roots from the transformed equations of motion to determine the aeroelastic stability of each feedback controlled configuration. The transformed aerodynamic forces are expressed as Padé approximates obtained from a least-squares-fitting scheme of sinusoidal generalized aerodynamic forces. The leading-edge flap and elastic displacement sensing seemed to be the best technique for controlling divergence speed of forward-swept wings. In the selected examples, an increase of divergence speed of approximately 25% is demonstrated. The flutter speed is increased by 30% with a trailing-edge flap and acceleration sensing. It is suggested that the structural designer separate flutter and divergence speeds as much as possible before beginning active control of these aeroelastic instabilities.

Nomenclature

$\{a\}$ = coordinate vector for modal coordinate system
$[A]$ = generalized aerodynamic force coefficient matrix
b = wing root semichord
k = reduced frequency
$[K]$ = generalized stiffness matrix
$[M]$ = generalized mass matrix
P_{nij} = Padé numerator coefficient
Q_n = Padé denominator coefficient
s = Laplace transform variable of time
U_∞ = freestream flow velocity
ϕ = trailing-edge flap deflection angle
χ = leading-edge flap deflection angle frequency of oscillation

I. Introduction

THE operation of high performance fighter aircraft with thin wings can be hampered by several aeroelastic instabilities. The most common of these structural catastrophic instabilities that can destroy the structure is aeroelastic flutter. Flutter problems can be found in both straight and aft-swept thin fighter wings but the aeroelastic divergence instability is almost nonexistent. Serious consideration is now being given to forward-swept wings for some fighter designs where divergence speed rather than flutter speed is usually the most critical instability, as discussed by Weisshaar.[1] This paper examines the use of active controls to increase the critical airspeeds at which both flutter and divergence occur in forward-swept wing designs.

The use of advanced composite materials is presently contemplated to overcome the problem of divergence in forward-swept wings. In these designs the deformation coupling of bending and torsion is controlled through the proper design of composites to postpone the divergence speed. This is done by properly orienting the number of plies and the fiber direction of the advanced composite material used in the construction of the wing box. This design technique called aeroelastic tailoring of the box structural material was used by Krone[2] as a method of increasing divergence speed of forward-swept wings. The present paper does not investigate problems associated with aeroelastic tailoring, but aeroelastic tailoring is used to provide examples that have their divergence and flutter speeds relatively close together. This close proximity of critical airspeeds is chosen so that the effects of the active control on both flutter and divergence can be monitored for a single wing design at the same time. Control of one aeroelastic instability should not cause an unacceptable deterioration of another aeroelastic instability.

II. Analysis

The method used to determine the aeroelastic stability of the wing configurations with and without feedback control is a root locus with the position of the roots in the complex plans as the indication of stability. These roots are the characteristic roots obtained from a Laplace transform of the equations of motion. The equations of motion, prior to the addition of the feedback control loops, describe the wing dynamics as

$$[M]\{\ddot{a}\} + [K]\{a\} = [A] \tag{1}$$

where $[M]$, $[K]$, and $[A]$ are the generalized mass, stiffness, and aerodynamic force matrices, respectively. The generalized stiffness matrix $[K]$ and generalized mass matrix $[M]$ are obtained using a set of generalized coordinates represented by several of the natural vibration mode shapes. These mode shapes are the lower frequency in-vacuum vibration modes of the wing. For initial calculations the first four modes are adequate to define the wing responses. For more precise calculations ten modes were necessary. The mass and stiffness

Presented as Paper 81-0637 at the AIAA Flight Simulation Technologies Conference, Long Beach, Calif., June 17-19, 1981; submitted June 30, 1981; revision received Dec. 21, 1981. This paper is declared a work of the U.S. Government and therefore is in the public domain.

*Assistant Professor, Department of Aeronautics, Captain USAF. Student Member AIAA.
†Professor and Director of Graduate Aerospace Engineering. Associate Fellow AIAA.

matrices in terms of spatial coordinates are developed using the Raleigh-Ritz method of the Wing Aeroelastic Synthesis Procedure TSO.[3] This is the most convenient method since TSO is used to aeroelastically tailor the wing boxes to produce the selected wing designs described below.

The generalized aerodynamic forces are obtained from Padé's approximations of sinusoidal forces obtained using the doublet-lattice aerodynamics.[4] This is a method similar to that suggested by Vepa[5] for subsonic flow. The Padé's approximations represent the transformed aerodynamic forces as polynomials in terms of the transformed variable s to relate generalized aerodynamic forces to the generalized coordinate in the complex plane. The power of s of the polynomials indicates which order of derivative of the generalized coordinate is matched with the polynomial coefficients. The polynomials used in Padé's approximates are of the form

$$\frac{P_{nij}\bar{s}^n + P_{n-1ij}\bar{s}^{n-1} + \ldots + P_{0ij}}{Q_2\bar{s}^2 + Q_1\bar{s} + 1} \tag{2}$$

where the subscripts indicate the jth generalized coordinate contribution to the ith generalized force. The value of n defines the order of the time derivative of the generalized coordinate. The real numbers P_{nij} are the numerator coefficients obtained by a least-squares-fitting process of the sinusoidal aerodynamic forces. The real numbers Q_2 and Q_1 are the coefficients of the denominator polynomial. The nondimensional form $\bar{s}$ of the transformed time variable s is used because of its association with the reduced frequencies of the sinusoidal aerodynamic forces used to define the Padé approximations. It is defined as

$$s = (U_\infty/b)\bar{s} \tag{3}$$

where b is the reference semichord and U_∞ is the freestream flow velocity. In order to convert the Padé approximations to polynomials in the variable s so that they represent aerodynamic force in the equations of motion, a value of freestream velocity and the reference chord is specified.

The approximation polynomials for each generalized aerodynamic force are obtained from sinusoidal aerodynamic forces. The doublet-lattice procedure was used to determine sinusoidal generalized aerodynamic forces for 20 reduced frequencies, k, in a range from zero to a value which ensured a good range of frequencies for the wing configuration to be examined. The reduced frequency k is defined as

$$k = \omega b/U_\infty \tag{4}$$

where ω is the frequency of the sinusoidal aerodynamic forces. The least-squares-fitting process allows one to obtain the coefficients of the Padé approximations to give the best representation of each generalized aerodynamic force in the complex s plane. This fitting process is accomplished in two stages. In the first stage one obtains a unique numerator polynomial and denominator polynomial for each element of the generalized aerodynamic force matrix. At this point, all of the denominator coefficients are then averaged to define a single common denominator for each element. This procedure means that the Padé approximate polynomials introduce only two extra apparent roots into the equations of motion rather than two extra roots for each element of the aerodynamic force matrix. In the second stage, one uses the least-squares-fitting process again to produce the numerator polynomials for each element of the generalized aerodynamic force matrix with a previously determined averaged denominator. The 20 sets of coefficients at the selected values of k allow one to obtain new numerator polynomials, but written in terms of the averaged denominator.

The active control system is composed of one or two aerodynamic flaps to provide a control force, one or two sensors located near the wing box tip to measure elastic motions, and simple gain amplifiers as compensators in the loop that connects the sensors and flaps. The flaps that provide aerodynamic force are located at the tip of the wing along the leading edge and trailing edge. Figure 1 shows the flap geometry and relative sizes. The flap rotation angles are also noted in Fig. 1. When only the trailing-edge flap is used for control, this is referred to as the flap A configuration. When only the leading edge flap is used, the configuration is noted as flap B. Two combinations of these flaps are defined as flap C and flap D configurations. The flap C configuration is such that the flaps are rotated through equal and positive deflection angles. The flap D configuration is such that the rotation angle of the leading edge flap is equal to but the negative of the trailing-edge flap. The actuator representation in the equations of motion is of the form

$$TF_{\text{act}} = 20/(s+20) \tag{5}$$

which is typical of the actuators used in modern fighter aircraft.

The sensors are located on the wing structural box near the wing tip. Sensor A has the location at the trailing edge of the wing box downstream from the junction of the leading-edge spar and tip wing rib. Sensor B is located at the junction of the leading-edge spar and tip wing rib. The sensor C configuration is sensor A and sensor B with their signals added together. The sensor D configuration is similar to that of sensor C except that the signal from sensor B is subtracted from sensor A.

The feedback of sensor information to the control surfaces are obtained through simple gain amplifiers that scale the sensor signals. An example of a typical feedback loop is shown in Fig. 2. The displacement and velocity sensing loops are similar. The types of sensors assumed in this study measure either elastic displacement, velocity, or accelerations. There is no attempt made at this time to model

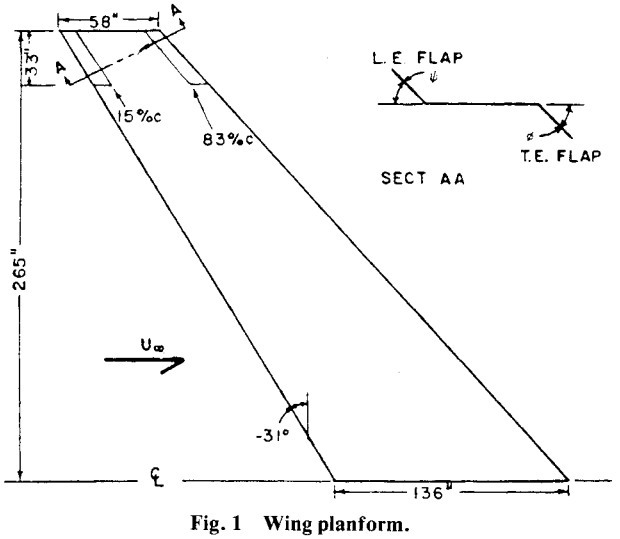

Fig. 1 Wing planform.

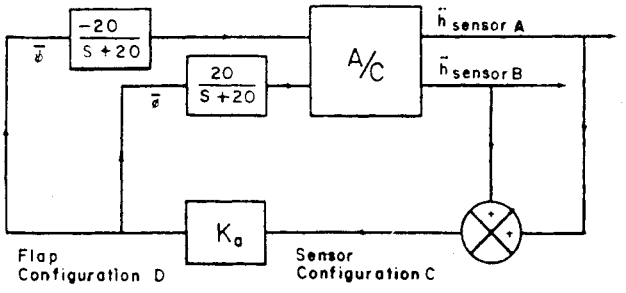

Fig. 2 Typical feedback loop for acceleration sensing.

mathematically the characteristics of particular devices as sensors. It is assumed that at selected sensor locations elastic displacements, velocities, and accelerations are available.

The addition to the equations of motion of aerodynamic forces due to the time-dependent actuation of the control surfaces is obtained with a second set of Padé approximations. These aerodynamic force approximations of the flaps are calculated separately from the previously calculated wing-only approximations of aerodynamic force. Again the doublet-lattice procedure is used to generate aerodynamic influence coefficients for each generalized coordinate due to sinusoidal control deflections of the flaps at 20 reduced frequencies. A least-squares-fitting process similar to the one used for the wing provides control surface forces in polynomials of $\bar{s}$.

$$\begin{Bmatrix} \\ \bar{A}_{\text{con}} \\ \\ \end{Bmatrix} = \begin{bmatrix} \bar{A}\bar{C}_{11} & \bar{A}\bar{C}_{12} \\ \bar{A}\bar{C}_{21} & \bar{A}\bar{C}_{22} \\ \vdots & \\ \bar{A}\bar{C}_{i1} & \bar{A}\bar{C}_{i2} \end{bmatrix} \begin{Bmatrix} \bar{\phi} \\ \\ \bar{\psi} \end{Bmatrix} \tag{6}$$

Each element uses the same denominator as that used by the wing aerodynamic forces:

$$\bar{A}\bar{C}_{ij} = \frac{PC_{3ij}\bar{s}^3 + PC_{2ij}\bar{s}^2 \ldots PC_{0ij}}{Q_2^2\bar{s} + Q_1\bar{s} + 1} \tag{7}$$

where element $\bar{A}\bar{C}_{ij}$ provides the generalized force contribution to coordinate i from control surface j. Thus the equations of motion in terms of the generalized coordinates and control deflections are

$$[[M]s^2 + [K]]\{\bar{a}\} = [\bar{A}]\{\bar{a}\} + [\bar{A}\bar{C}]\begin{Bmatrix} \phi \\ \bar{\psi} \end{Bmatrix} \tag{8}$$

When the simple feedback control is included in the equations of motion, relating measurements of motion to control deflections, the equations of motion become functions of the generalized coordinates $\bar{a}$ only. In this formulation the critical roots of the equations at selected velocities and/or gain values can be obtained from standard eigenanalyses. A plot of these root locations, as the freestream velocity U_∞ or a gain value such as Ka is varied, provide the root loci used to determine the aeroelastic stability of the wing.

The stability of the wings for flutter and divergence is determined from the root locations at various velocities or feedback gains with respect to their position relative to the imaginary axis. The aeroelastic divergence condition occurs when a nonoscillatory root (zero imaginary part) crosses the imaginary axis from the negative to the positive real axis. A root of the equations of motion is thus determined which provides a response in the time domain of monotonic increasing displacement without oscillatory content. If the root crossing the imaginary axis has a nonzero imaginary part, divergent oscillatory motion is predicted and flutter is defined. In the time domain the monotonic increasing displacement has then superimposed on it the oscillatory content corresponding to the flutter frequency. Here only simple control relationships are used between the sensors and the resulting flap rotations. These simple control laws were used to examine the basic relations between wing deformation, resulting flap motion, and the wing aeroelastic instabilities. In a more practical sense the use of optimal control techniques is suggested for future studies.

III. Selected Wing Examples

It is desired to investigate active control of both flutter and divergence speeds of forward-swept wings. To investigate control of both aeroelastic instabilities two different wings are considered. The first wing has a divergence speed less than the flutter speed and is designated as the case 1 wing. The second wing has a flutter speed less than the divergence speed and is designated as the case 2 wing. In both cases, the difference between the flutter and divergence speeds is small enough so that the variation of one of the aeroelastic instabilities may be observed while the other aeroelastic instability is being controlled. Both the case 1 wing and case 2 wing have the same planform and structural geometry as shown in Fig. 1. The structure of the two wings differ only in the number of plys and fiber orientations of graphite/epoxy materials from which the skin is manufactured. The difference in skin composition accounts for the difference in the flutter and divergence speeds of the two wings.

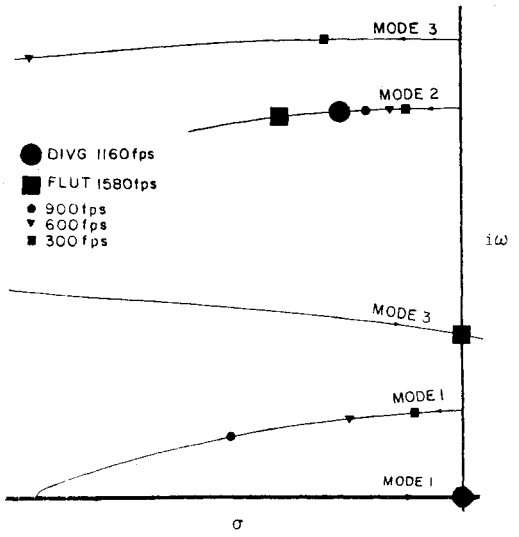

Fig. 3 Velocity root locus for case 1 wing, no feedback control, ten-mode basis.

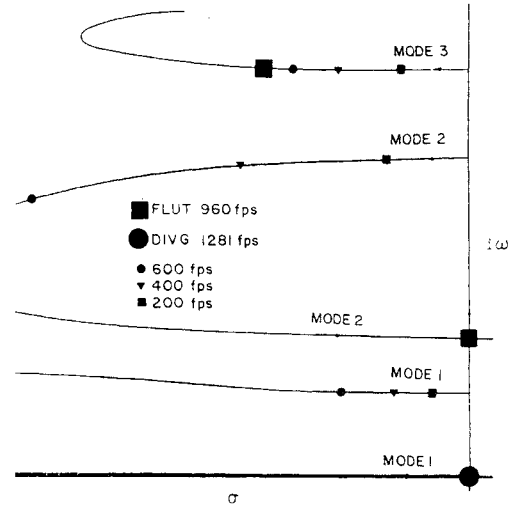

Fig. 4 Velocity root locus for case 2 wing, no feedback control, ten-mode basis.

The velocity root loci of the case 1 and case 2 wings without feedback control are shown in Figs. 3 and 4. The wing response was represented with ten modes in the calculations but only the loci of roots corresponding to the first three modes are shown in Figs. 3 and 4. The most critical flutter and divergence speeds are determined from Figs. 3 and 4 as the crossing of the loci with the imaginary axis for the least value of velocity for both oscillatory and nonoscillatory loci.

Figure 3 shows the movement of the three roots with the lowest in-vacuum frequencies for case 1. The loci are obtained by increasing in small increments the value of U_∞ in the

equations of motion from 0 to 2010 ft/s. At each increment, eigenvalues are obtained and plotted. Note that modes 1-3 (roots 1-3) start at the imaginary axis at zero airspeed and initially pick up damping as the airspeed increases. Mode 1 loses its oscillatory content, sends one root in the positive real direction, and one in the negative real direction. At an airspeed of 1160 ft/s one of the roots from mode 1 crosses the imaginary axis and defines a critical divergence condition. As the airspeed continues to increase, mode 3 drops in frequency, begins to lose its positive damping, and crosses the imaginary axis at 1580 ft/s. This defines the most critical flutter airspeed. This graphical technique is used to investigate all of the feedback control configurations in this study.

Figure 4 presents the root locus of the case 2 wing without active feedback. Again, three of the loci for the ten modes used in the calculations are shown as the airspeed velocity is incremented from 0 to 2010 ft/s. In a similar manner to Fig. 3, mode 1 defines a critical divergence airspeed of 1281 ft/s. In this case however, mode 2 defines a flutter airspeed of only 960 ft/s, making this aeroelastic instability the most critical for case 2. As feedback is added to both case 1 and case 2, Figs. 3 and 4 can be used as references to observe the changes in the root loci of case 1 and case 2, both in critical airspeed and modal participation of the instabilities.

IV. Results

To determine the best combinations of control surfaces and sensors, gain-root loci are obtained for each combination of sensors and control surfaces. These root loci are obtained at the critical value of the aeroelastic instability determined for the two wing cases being studied. By generating these roots at various values of gain settings while holding the velocity constant, a gain-root loci is obtained. The wing response for investigation of controlling aeroelastic instabilities is represented by four natural modes as opposed to ten modes for the uncontrolled wings.

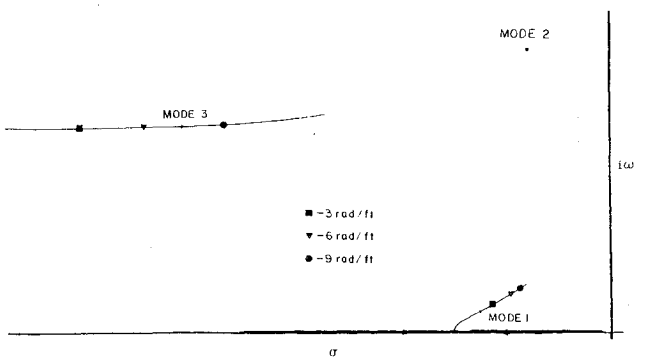

Fig. 5 Gain-root locus for case 1 wing, velocity fixed at 1160 ft/s, sensor D/flap B, four-mode basis.

Wing Case 1

Gain root loci using displacement sensing provided a sensor/control surface combination that seemingly could improve the critical divergence speed for the case 1 wing. The 16 combinations of control surface and displacement sensors were examined both with negative and positive gain. These resultant root loci for all sensor and flap combinations showed both the improvement capability and the degradation possibilities of elastic displacement sensing. In all cases positive gain from the displacement lowered the critical divergence velocity.

The sensor D/flap B combination yields the largest increase of the divergence velocity beyond the uncontrolled divergence velocity of case 1. Figure 5 shows the gain root locus for this feedback control combination. Note that several values of gain have their associated root locations marked. As was true for other feedback combinations investigated, a drop in flutter speed occurs with the addition of feedback compensation for the increase of divergence speed. The flutter instability is associated with mode 2 while the divergence instability is associated with mode 1. The degradation in the critical flutter velocity that occurs with increased negative gain progressed slowly enough to allow large improvement in the critical divergence velocity.

Three velocity root loci using displacement sensing together with the sensor D/flap B combination are presented in Figs. 6-8. Figures 6-8 demonstrate the increase in divergence velocity as the gain value is varied. The velocity root locus for a gain value of -3 rad/ft is shown in Fig. 6. Figure 6 indicates that the flutter instability is associated with mode 3 and the speed at which a crossing of the imaginary occurs is 1480 ft/s. This represents a decrease in flutter speed of 100 ft/s from the wing flutter speed without control. Further, the divergence instability is associated with mode 1 and is determined to be 1345 ft/s, which represents an increase of 183 ft/s beyond the divergence speed of the uncontrolled wing. The gain is now increased to a value of -6 rad/s and the velocity root loci is shown in Fig. 7. When the gain is increased to -6 rad/s the crossing of the imaginary axis for mode 1 and mode 3 occurs at identical velocities; thus the flutter and divergence

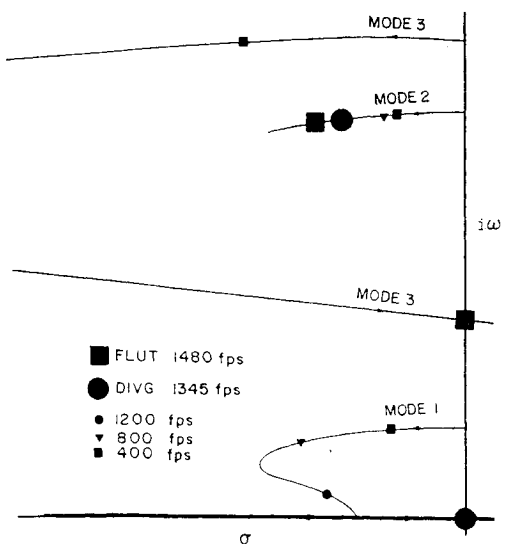

Fig. 6 Velocity root locus for case 1 wing, displacement gain; −3 rad/ft, sensor D/flap B, four- mode basis.

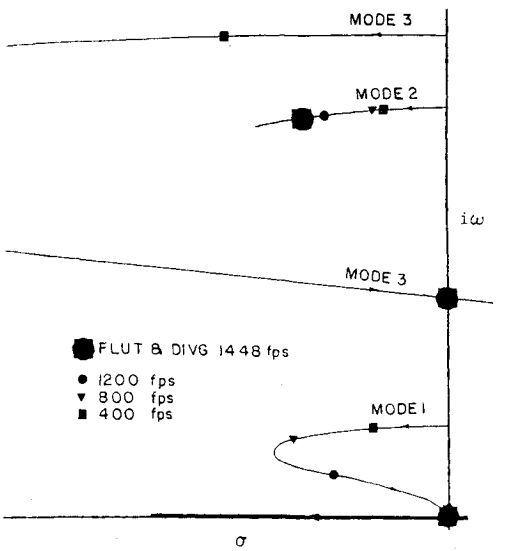

Fig. 7 Velocity root locus for case 1 wing, displacement gain; −6 rad/ft, sensor D/flap B, four-mode basis.

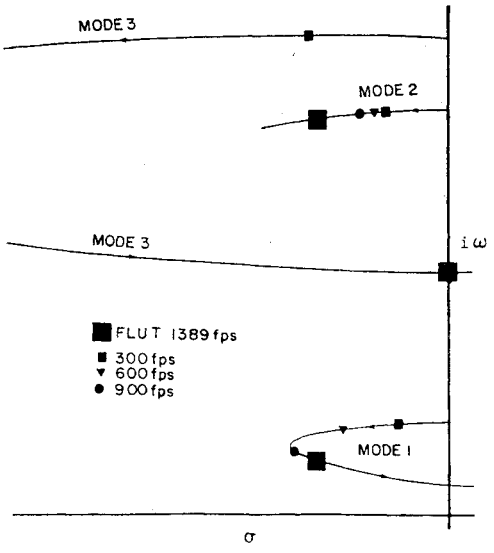

Fig. 8 Velocity root locus for case 1 wing, displacement gain; −9 rad/ft, sensor D/flap B, four-mode basis.

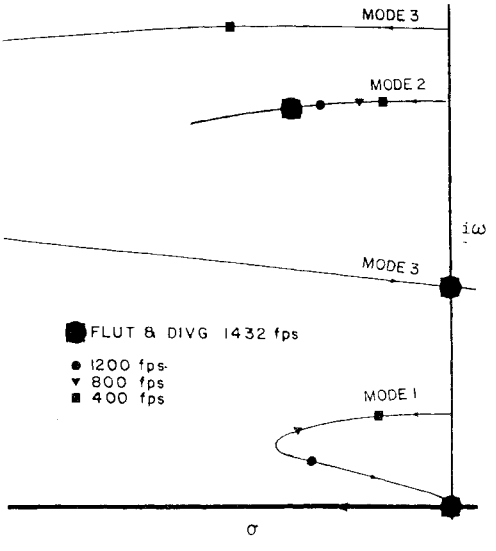

Fig. 9 Velocity root locus for case 1 wing, displacement gain; −6 rad/ft, sensor D/flap B, ten-mode basis.

velocities are the same. This represents a 25% increase in divergence speed together with a reduction of 10% in flutter speed as compared to the aeroelastic instability speeds without control. The value of gain of −6 rad/s represents the best possible gain value, for any further gain increase would reduce the flutter speed to less than the divergence speed, requiring a different control feedback loop. Figure 8 shows the velocity root loci when the gain is increased to −9 rad/s. This increase in gain causes mode 1 to cross the imaginary axis with an oscillatory content; thus the divergence instability of mode 1 has been converted to a flutter instability. This change is due to the oscillatory content now present in mode 1 at this critical airspeed. The most critical flutter speed, however, is still defined by mode 3 at 1389-ft/s airspeed. This lowest critical airspeed is much lower than that found when the gain was −6 rad/s. Therefore a gain value of −6 rad/s defines the displacement sensing with the best compromise in raised divergence velocity with lowered flutter velocity.

The trade between flutter and divergent speed illustrates two points. First, even more improvement in divergence speed would have been available if the original uncontrolled flutter speed had been greater. If this original flutter speed had been greater, a larger value of gain could have been used, postponing any aeroelastic instability until the crossing of mode 1 as an oscillatory instability at that greater airspeed. Since most forward-swept wings have very large flutter speeds, probably more improvement can be expected than has been demonstrated with the selected case 1 wing.

If feedback control is contemplated as a means of increasing divergence, perhaps the best uncontrolled wing design would result from a larger spread in critical airspeeds rather than just large critical airspeeds. This would allow the feedback control system to increase the divergence velocity to a higher velocity which equals the decreased flutter speed.

The sensitivity of control using the sensor D/flap B combination to the number of modes used to represent wing response was investigated. A velocity root loci is shown in Fig. 9, where ten natural modes rather than four modes are used to represent wing response. The addition of more modes makes subtle changes in both the aerodynamic forces, because of the averaging done for the Padé denominator polynomial, and the structural stiffness, because of slight movements of nodal lines. Only the first three modes are shown even though ten modes were used in all calculations. With this ten-mode representation one can determine the flutter and divergence speed as 1432 ft/s rather than 1448 ft/s obtained with four modes. This is a variation of less than 1% in velocity.

When velocity sensing rather than displacement sensing is used for the case 1 wing the controlling of divergence speed is not successful. The same combinations of flap locations and sensor locations are used as in the displacement sensing studies earlier. However with the 32 flap, sensor, and gain sign combinations possible, no successful combination using a gain range of 0-15.55 rad s/ft improved the divergence speed. At the same time many degraded the flutter speed. The third type of sensor used in this investigation measured elastic acceleration. The combinations of flap and sensor locations are again the same as used in the displacement and velocity studies; however, no combination of flaps and sensors improved the divergence speed, while many degraded the flutter speed.

Of all the control configurations that were considered, only certain displacement sensing combinations improved the airspeed at which divergence occurred for the case 1 wing. Owing to the location and coupling of the sensors, the deformation that proves useful to measure is the elastic angle of attack change. Comparing the elastic angle change, the sign of the feedback gain, and the geometry of the leading-edge flap, feedback control appears to momentarily change the lift at the wing tips. This is done by the camber change that the deformed leading-edge flap introduces into the tip wing section. As an elastic deformation begins to develop, the aerodynamic force at the tip is increased, causing divergence. The feedback control sensor-flap combination used for case 1 wing, results in a reversal of aerodynamic force at the wing tip, which results in a changed deformation shape of the wing and delays the onset of the divergence condition. This is a different mechanism of improving stability than is commonly used for flutter instabilities. Increasing loss of energy to the airstream by increasing the artificially created damping is common to flutter active suppression systems. The fact that the divergence instability has no oscillatory content requires a direct modification of the applied forces that are deflection dependent.

Wing Case 2

The case 2 example of the forward-swept wing requires an improvement in flutter speed rather than divergence. The low value of divergence speed does allow the monitoring of the stabilizing feedback control aimed at flutter on the divergence instability. The same sensor/flap configurations and type of sensors are used for case 2 as were used for the case 1 study.

In employing displacement sensing for case 2, only negative feedback is used since positive feedback greatly reduced the

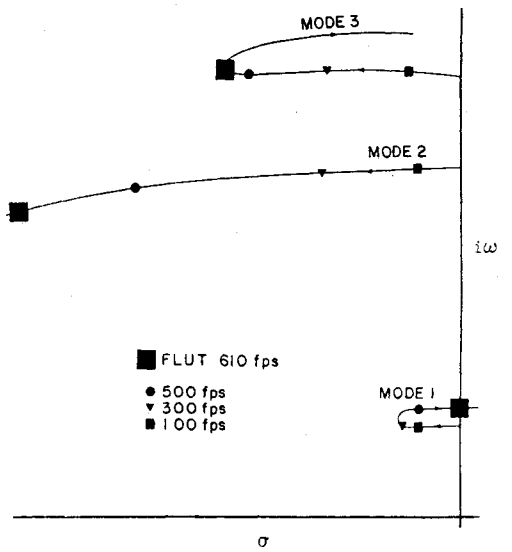

Fig. 10 Velocity root locus for case 2 wing, displacement gain; −15 rad/ft, sensor A/flap B, four-mode basis.

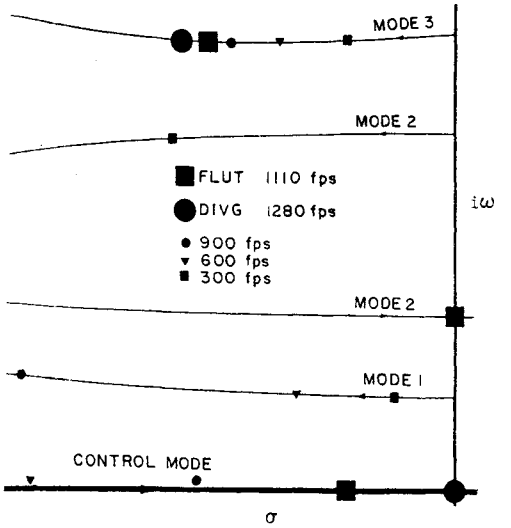

Fig. 11 Velocity root locus for case 2 wing, velocity gain; 0.15 rad s/ft, sensor D/flap D, four-mode basis.

divergence velocity in the case 1 study. No successful displacement sensing feedback control loop could be found to increase the flutter velocity for case 2 wing. Either both the flutter and divergence mode are driven to lower critical airspeeds or divergence rapidly drops with only a small improvement in flutter. The displacement sensing, resulting in degradation of the divergence root, is shown in Fig. 10. The velocity root locus of mode 1 shows that the feedback control has caused mode 1 to go unstable at a low airspeed (610 ft/s) as a flutter instability rather than as a divergence instability. Usually mode 1 is the mode associated with the divergence instability and intersects the real axis at a greater airspeed with no oscillatory component at the intersection. Thus displacement sensing with control has forced a lower flutter speed than the case 2 wing has without feedback control.

Velocity sensing rather than displacement sensing does seem to provide an improvement of flutter velocity for the case 2 wing. In employing velocity sensing, no change is observed of the divergence velocity and only the modes with oscillatory content are changed with controls. A velocity root locus for sensor D/flap D configuration using velocity sensing and a gain of 0.15 rad s/ft gain is shown in Fig. 11. Here the flutter speed is determined from the crossing of mode 2 with the imaginary axis at a velocity of 1110 ft/s, representing an increase of 150 ft/s beyond the uncontrolled flutter speed of case 2 wing. Note also that the divergence condition associated with mode 1 occurs at a velocity of 1280 ft/s, which agrees with the uncontrolled divergence speed of case 2 wing.

Acceleration sensing seemed to offer the greatest improvement of flutter speed beyond the uncontrolled case 2 wing. In Fig. 12 a velocity root loci is shown of sensor D/flap A using a gain of -0.05 rad s^2/ft and a four-mode representation of wing response. Note that the divergence condition is uneffected by feedback control and mode 1 still defines divergence at 1280 ft/s. However, mode 2, the uncontrolled flutter mode, now does not cross the imaginary axis and the flutter instability no longer exists at these airspeeds. Flutter is postponed until a much higher flow speed. Eventually mode 2 does go unstable at about 1815-ft/s freestream airspeed. Since the divergence velocity now represents the lowest critical airspeed, the improvement in airspeed for the most critical aeroelastic condition is about 32%. In this case we have converted an unacceptable flutter instability to an acceptable divergence instability through control. This seems to suggest that even larger values of improvement might be possible if the original uncontrolled divergence speed is greater. The velocity root loci shown in

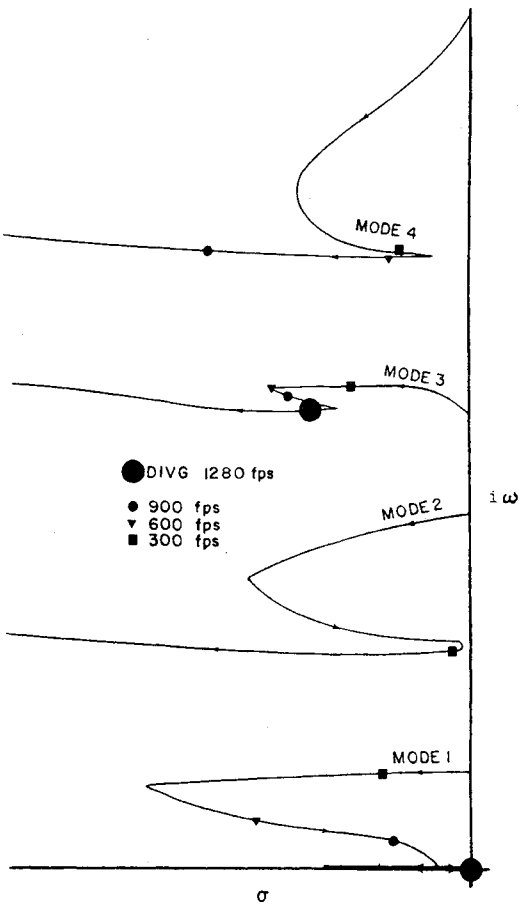

Fig. 12 Velocity root locus for case 2 wing, acceleration gain; −0.05 rad s^2/ft, sensor D/flap A, four-mode basis.

Fig. 12 indicates additionally that both modes 2 and 4 move very close to the imaginary axis, which means small parameter variations could be quite disastrous. Mode 4 moves to the imaginary axis at a velocity of 450 ft/s, which is a highly responsive situation but nonetheless still stable. Some caution must be displayed in obtaining the velo ity root loci for the control combinations. In particular some sensitivity of the velocity root loci can be attributed to the number of modes used to represent wing response and the use of an averaging method to represent aerodynamic force with Padé polynomials.

V. Conclusions and Discussion

Feedback control of two selected forward-swept wing configurations has been used to increase the critical velocity at which divergence or flutter instabilities occur. The divergence speed was increased using elastic displacement sensing with the case 1 wing, which had an uncontrolled divergence speed less than the flutter speed. Similarly, the flutter speed was increased using elastic acceleration sensing with the case 2 wing, which had an uncontrolled flutter speed less than the divergence speed. In both cases the increase in velocity of the controlled aeroelastic instabilities occurred with some reduction of velocity of the other aeroelastic instability. Specifically the ability to deal with the nonoscillatory divergence instability using an instantaneous aerodynamic force modification shows promise. However, since elastic displacement will occur as a normal result of aircraft subcritical aerodynamic loads, the ability to distinguish and identify the divergence critical displacements will require further investigation of actual aircraft sensor designs.

If forward-swept wings are to be constructed from metals rather than composite materials, perhaps the use of active control techniques discussed herein could be employed as a means of increasing wing divergence speed. Thus active control of aeroelastic instabilities could serve as an alternative to aeroelastic tailoring for increasing the divergence speed of forward-swept wings with reasonable wing weights. The direction taken in preliminary structural design may have to be modified by the prospect of using these feedback control techniques. An overall better wing may result, if the primary objective in structural design is to spread the velocities of these two aeroelastic instabilities rather than grouping them together just outside the operating envelope of the aircraft. This would allow feedback control to deal with the critical instability without unacceptable degradation of another instability in close proximity.

References

[1] Weishaar, T.A., "Aeroelastic Stability and Performance Characteristics of Aircraft with Advanced Composite Swept Forward Wing Structures," AFFDL-TR-78-116, Sept. 1978.

[2] Krone, N.J. Jr., "Divergence Elimination with Advanced Composites," AIAA Paper 75-1009, 1975.

[3] Lynch, R.W., Rogers, W.A., and Braymen, W.W., "Aeroelastic Tailoring of Advanced Composite Structures for Military Aircraft," AFFDL-TR-76-100, Feb. 1978.

[4] Giesing, J.P., Kalman, T.P., and Rodden, W.P., "Subsonic Unsteady Aerodynamics for General Configurations," AFFDL-TR-71-5, April 1972.

[5] Vepa, R., "On the Use of Padé Approximants to Represent Unsteady Aerodynamic Loads for Arbitrary Small Motions of Wings," AIAA Paper 76-17, Jan. 1976.